PHYSICAL REVIEW D **88,** 015019 (2013)

Phenomenology of partially composite standard model

Tomohiro Abe[1] and Ryuichiro Kitano[1,2]
[1]*KEK Theory Center, Tsukuba 305-0801, Japan*
[2]*The Graduate University for Advanced Studies (Sokendai), Tsukuba 305-0801, Japan*
(Received 14 May 2013; published 12 July 2013)

We propose a model to describe the low energy physics of the partially composite Standard Model, in which the electroweak sector in the Standard Model is weakly coupled to some strong dynamics. The vector resonances in the strong sector are introduced as the effective degrees of freedom, W' and Z', which mixes with the W and Z bosons through the electroweak symmetry breaking. Through the coupling to the strong sector, the Standard Model Higgs boson becomes partially composite, and its properties are modified. We study the constraints from the electroweak precision data and direct searches of W' and Z' at the LHC expriments, and discuss the effects on the production/decay properties of the Higgs boson.

DOI: 10.1103/PhysRevD.88.015019 PACS numbers: 12.60.Cn, 12.60.−i, 12.60.Fr, 14.70.Pw

I. INTRODUCTION

The discovery of the Higgs boson at 125 GeV and the measurements of its production and decay rates strongly support the picture of the weakly coupled Higgs mechanism for the electroweak symmetry breaking. It is then important to (re)consider the origin of the Higgs field and its potential. The fact that the Higgs boson mass is much smaller than $4\pi v$, where $v = 246$ GeV, tells us that the dynamics behind electroweak symmetry breaking has a very good description in terms of the linear sigma model.

Not only from its mass, constraints from flavor changing neutral current and CP violating processes suggest that the picture of the elementary Higgs field continues to be valid up to a much higher than $\mathcal{O}(10)$ TeV energy scale. This may be indicating that the physics to reveal the origin of the Higgs field (which is possibly string theory) is out of the reach of the LHC experiments.

Although the picture of the weakly coupled elementary Higgs field may be valid up to a very high energy scale, it can be a different question what generates the Higgs potential to drive the electroweak symmetry breaking, and what sets the scale of the vacuum expectation value (VEV), $v = 246$ GeV. For example, one can consider new particles or dynamics at a TeV energy scale and the Higgs field couples to it so that the Higgs potential is generated. If the elementary Higgs field is weakly coupled to the TeV scale dynamics, the Higgs field naturally obtains the potential to explain $v = 246$ GeV, while the picture of the elementary Higgs fields remains valid much above the TeV energy scale. The coupling to the dynamical sector generically causes mixing between the elementary Higgs and some (composite) operators in the dynamics, making the observed Higgs boson a partially composite particle. The picture that the Higgs field is weakly coupled to a TeV dynamics is particularly motivated in supersymmetric models where the simplest model, the minimal supersymmetric standard model, predicts the Higgs boson to be lighter than the Z boson at tree level. The partial compositeness explains why the Higgs boson is heavy while the new dynamics can possibly provide a mechanism to address the naturalness problem in supersymmetric models [1–11]. See also Refs. [12–14] for earlier proposals of TeV scale supersymmetric dynamics with elementary Higgs fields. For more ambitious proposals to break supersymmetry by the same dynamics, see Refs. [15–17]. In these works, it has been assumed that the dynamics rather than the Higgs VEV is the main source for the electroweak symmetry breaking. Although such a situation is now severely constrained by the electroweak precision tests, the framework is still an attractive possibility by focusing on a different region of the parameter space where the Higgs VEV is the main contribution to the W boson mass. For proposals and studies of nonsupersymmetric models, see [18–20].

In the TeV dynamics we consider, there should be Higgs-like operators that can couple to the elementary Higgs field. This indicates that the dynamical sector has $\mathrm{SU}(2)_L \times \mathrm{U}(1)_Y$ as a part of the global symmetry just as in QCD. We, therefore, expect that there are resonances, W' and Z', which couple to the $\mathrm{SU}(2)_L \times \mathrm{U}(1)_Y$ current, such as the ρ meson in QCD. Without specifying the actual dynamics, one can construct an effective theory of vector resonances W' and Z' as the gauge bosons of spontaneous broken gauge theory analogous to the hidden local symmetry [21–24] in QCD. In the partially composite Higgs framework, we expect that the vector resonances appear at a TeV energy scale, which is within the reach of the LHC experiments.

In this paper, we construct an effective theory of the W'/Z' sector that couples to the Standard Model Higgs boson. The Higgs operators that give masses to W'/Z' can mix with the Standard Model Higgs boson, and trigger the electroweak symmetry breaking. We first examine the constraints from the electroweak precision tests to see which region of the parameter space is allowed. We then reinterpret the results of the searches for W'/Z' in the sequential Standard Model at the LHC to the constraints on W'/Z' in the model. We see that the LHC experiments give stronger constraints than the precision tests in some parameter regions. The properties of the Higgs boson are

modified by the partial compositeness. We examine whether such a modification is allowed by the present data. For example, we find that there are parameter regions where the strong sector components of the Higgs boson is as large as 30%.

Our work is closely related to Ref. [25] where phenomenology of the models with W'/Z' is studied, motivated by the framework of the Higgs boson as a pseudo Nambu-Goldstone boson [26,27]. There, a scalar particle is added to the nonlinear sigma models of W'/Z', and the constraints from the electroweak precision measurements and from the LHC data are discussed. We, on the other hand, construct a linear sigma model to describe W'/Z' resonances and couple the Higgs field to it. Compared to the work in Ref. [25], we do not need to assume relations among parameters motivated by the restoration of the perturbative unitarity, and all the physical quantities are, in principle, calculable. In the linear sigma model, we find that there is an important parameter, r, which describes the parity violation in the dynamical sector. We see that the constraints from the precision measurements prefer a large parity violation, and in such parameter regions, the searches for W'/Z' at the LHC experiments become more important.

II. MODEL

A. Lagrangian

We construct a model to describe the W' and Z' bosons as the gauge bosons of new SU(2) gauge interactions. The full gauge symmetry is, therefore, $\mathrm{SU}(3) \times \mathrm{SU}(2)_0 \times \mathrm{SU}(2)_1 \times \mathrm{U}(1)_2$, where SU(3) is QCD, and remaining parts are the electroweak sector. The $\mathrm{SU}(2)_1$ gauge factor is the one that is analogous to the hidden local symmetry in QCD, and thus we assume its gauge coupling is much larger than those of $\mathrm{SU}(2)_0$ and $\mathrm{U}(1)_2$. We also assume that all the quarks and leptons are elementary. They do not carry $\mathrm{SU}(2)_1$ charges although they eventually couple to W'/Z' through mixing. The left-handed fermions are fundamental representations of $\mathrm{SU}(2)_0$, and the right-handed fermions are singlet. All the fermions have appropriate $\mathrm{U}(1)_2$ charges to reproduce the electric charges.

Three Higgs fields, H_1, H_2, and H_3, are introduced for the electroweak symmetry breaking. The VEVs of H_1, H_2, and H_3 break $\mathrm{SU}(2)_0 \times \mathrm{SU}(2)_1$, $\mathrm{SU}(2)_1 \times \mathrm{U}(1)_2$, and $\mathrm{SU}(2)_0 \times \mathrm{U}(1)_2$, respectively.[1] The H_1 and H_2 fields represent the condensations in the dynamical sector. Their VEVs give masses to W' and Z'. On the other hand, H_3 is the elementary Higgs boson in the Standard Model. Through the Higgs potential, the Standard Model Higgs field H_3 mixes with "hadrons" (H_1 and H_2) in the dynamical sector, and thus becomes partially composite. All the fields except gauge bosons are summarized in Table I. We show a schematic description of the model in Fig. 1 by using the moose notation [29]. The model is simply the Standard Model added by H_1, H_2, and the $\mathrm{SU}(2)_1$ gauge fields.

TABLE I. Quantum numbers of the Higgs and matter fields.

Fields	$\mathrm{SU}(2)_0$	$\mathrm{SU}(2)_1$	$\mathrm{U}(1)_2$	$\mathrm{SU}(3)_c$
H_1	**2**	**2**	0	1
H_2	**1**	**2**	1/2	**1**
H_3	**2**	**1**	1/2	**1**
Q_L	**2**	**1**	1/6	**3**
L	**2**	**1**	−1/2	**1**
u_R	**1**	**1**	2/3	**3**
d_R	**1**	**1**	−1/3	**3**
e_R	**1**	**1**	−1	**1**

Models such as in Refs. [1,3,11] provide concrete examples of the UV completion of this model. As one can see from the moose diagram, the model has a structure of the Seiberg dual picture of supersymmetric QCD, where the $\mathrm{SU}(2)_1$ factor is the magnetic gauge group, H_1 and H_2 are dual squarks, and H_3 is the meson field. In general, if there is an effective description of the system of W', Z', and the Higgs field, where W' and Z' are much lighter than the UV cutoff scale, our model is the minimal model to describe it since the massive vector bosons must be introduced as gauge fields along with appropriate Higgs fields to give masses to them.

Each Higgs field contains four real scalars, and six of them are eaten by the gauge bosons. So the six ($= 4 \times 3 - 6$) scalars remain as physical degrees of freedom. This is the minimal model for the partially composite Higgs boson. Note that if we did not consider partial compositeness with the same gauge symmetry, two Higgs fields would be enough to break the symmetry [30–34]. In such models, physical charged scalar bosons are absent.

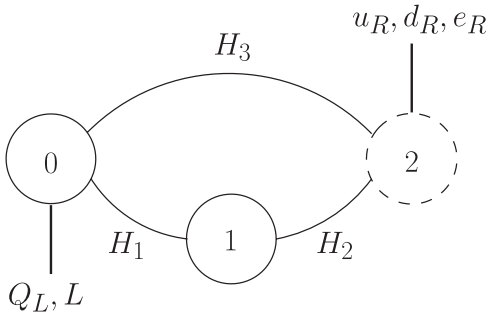

FIG. 1. A schematic model description by the moose notation: The circles represent gauge symmetries. The dashed one is U(1) gauge symmetry. The lines that connect two circles are the Higgs fields and break the symmetry they connect. The lines attached to the zeroth and second sites represent left- and right-handed fermions, respectively. We assume that H_1, H_2, and the first site belong to the dynamical sector.

[1]The same symmetry breaking pattern is studied in Ref. [28] in the top triangle moose model.

However, in our setup, there are charged and CP-odd scalars as well as CP-even scalars. The existence of the charged and CP-odd scalar bosons are a distinctive feature of our model compared to other SU(2) models.

The models without H_3 are strongly constrained from the S/T parameters. It has been observed that such constraints get significantly weaker when the Standard Model (SM) fermions are charged under $\mathrm{SU}(2)_1$, i.e., where SM fermions are composite [35–39]. Such models, if they exist, are subject to the constraints from searches for flavor changing neutral current (FCNC)/CP nonconservations. In this paper, we take a more conservative approach that the SM fermions are all elementary and there is a fundamental Higgs field that gives masses to fermions through the Yukawa intereactions, so that the well-tested Cabibbo-Kobayashi-Maskawa theory is not modified.

The Lagrangian is given as follows:

$$\mathcal{L}^{\mathrm{gauge}} = -\frac{1}{4}\sum_{a=1}^{3} W_{0\mu\nu}^{a} W_{0}^{a\mu\nu} - \frac{1}{4}\sum_{a=1}^{3} W_{1\mu\nu}^{a} W_{1}^{a\mu\nu} - \frac{1}{4} B_{\mu\nu} B^{\mu\nu}, \tag{1}$$

$$\mathcal{L}^{\mathrm{Higgs}} = \mathrm{tr}((D_\mu H_1)^\dagger D^\mu H_1) + \mathrm{tr}((D_\mu H_2)^\dagger D^\mu H_2) + \mathrm{tr}((D_\mu H_3)^\dagger D^\mu H_3) - V(H_1, H_2, H_3), \tag{2}$$

$$\mathcal{L}^{\mathrm{matter}} = \sum_i (\bar{Q}_L^i i\gamma^\mu D_\mu Q_L^i + \bar{u}_R^i i\gamma^\mu D_\mu u_R^i + \bar{d}_R^i i\gamma^\mu D_\mu d_R^i + \bar{L}^i i\gamma^\mu D_\mu L^i + \bar{e}_R^i i\gamma^\mu D_\mu e_R^i), \tag{3}$$

$$\mathcal{L}^{\mathrm{Yukawa}} = -\sum_{i,j} \bar{Q}_L^i H_3 \begin{pmatrix} y_u^{ij} & 0 \\ 0 & y_d^{ij} \end{pmatrix} \begin{pmatrix} u_R^j \\ d_R^j \end{pmatrix} - \sum_i \bar{L}^i H_3 \begin{pmatrix} 0 & 0 \\ 0 & y_e^i \end{pmatrix} \begin{pmatrix} 0 \\ e_R^i \end{pmatrix} + (\mathrm{H.c.}), \tag{4}$$

where i and j are generation indices. The Higgs fields are given by[2]

$$H_1 = \langle H_1 \rangle + \frac{1}{2}\left(h_1 + i\sum_{a=1}^{3} \tau^a \pi_1^a\right), \tag{5}$$

$$H_2 = \langle H_2 \rangle + \frac{1}{2}\left(h_2 + i\sum_{a=1}^{3} \tau^a \pi_2^a\right), \tag{6}$$

$$H_3 = \langle H_3 \rangle + \frac{1}{2}\left(h_3 + i\sum_{a=1}^{3} \tau^a \pi_3^a\right), \tag{7}$$

where τ^a denote the Pauli matrices, and $T^a = \tau^a/2$. Note that we take the matrix notation for the Higgs fields. All the Higgs fields are under the constraint

$$\tau^2 H_i^* \tau^2 = H_i, \qquad i = 1, 2, 3. \tag{8}$$

The Higgs potential, $V(H_1, H_2, H_3)$, is

$$V(H_1, H_2, H_3) = \mu_1^2 \mathrm{tr}(H_1 H_1^\dagger) + \mu_2^2 \mathrm{tr}(H_2 H_2^\dagger) + \mu_3^2 \mathrm{tr}(H_3 H_3^\dagger) \tag{9}$$

$$+ \kappa\, \mathrm{tr}(H_1 H_2 H_3^\dagger) \tag{10}$$

$$+ \lambda_1 (\mathrm{tr}(H_1 H_1^\dagger))^2 + \lambda_2 (\mathrm{tr}(H_2 H_2^\dagger))^2 + \lambda_3 (\mathrm{tr}(H_3 H_3^\dagger))^2 \tag{11}$$

$$+ \lambda_{12}\, \mathrm{tr}(H_1 H_1^\dagger)\, \mathrm{tr}(H_2 H_2^\dagger) + \lambda_{23}\, \mathrm{tr}(H_2 H_2^\dagger)\, \mathrm{tr}(H_3 H_3^\dagger) + \lambda_{31}\, \mathrm{tr}(H_3 H_3^\dagger)\, \mathrm{tr}(H_1 H_1^\dagger). \tag{12}$$

Here all coefficients can be taken as real numbers. Note that

$$(\mathrm{tr}(H_1 H_2 H_3^\dagger))^* = \mathrm{tr}(H_1 H_2 H_3^\dagger). \tag{13}$$

We can also write the following term:

$$\mathrm{tr}\,(H_1 H_2 \tau^3 H_3^\dagger). \tag{14}$$

This term can be eliminated by a field redefinition of H_2.[3] Since the vacuum should respect $\mathrm{U}(1)_{\mathrm{em}}$ symmetry, the Higgs VEVs, $\langle H_1 \rangle$, $\langle H_2 \rangle$, and $\langle H_3 \rangle$, should be diagonal. In addition, we can always take $\langle \pi_i^3 \rangle = 0$ by the gauge transformations. So we work in a basis in which all the Higgs VEVs are proportional to the identity matrix:

$$\langle H_1 \rangle = \frac{v_1}{2}, \qquad \langle H_2 \rangle = \frac{v_2}{2}, \qquad \langle H_3 \rangle = \frac{v_3}{2}, \tag{15}$$

where v_1, v_2, and v_3 are real and positive numbers. We introduce v and r as

$$v^2 = \frac{v_1^2 v_2^2}{v_1^2 + v_2^2} + v_3^2, \qquad r = \frac{v_2}{v_1}. \tag{16}$$

As we will discuss in Sec. III A, the relation between v and the Fermi constant is the same as the one in the Standard Model, $v^2 = (\sqrt{2} G_F)^{-1}$, so $v \sim 246$ GeV. The parameter $1 - v_3^2/v^2$ measures the size of the contribution to the electroweak symmetry breaking from the dynamical sector. The ratio r is an important parameter in later discussion. In QCD-like technicolor theories, $r = 1$ is predicted due to the parity conservation. As we see later, the model with $r = 1$ is severely constrained by the electroweak precision tests.

The limits $r = 0$ and $r \to \infty$ are other special points where parity ($H_1 \leftrightarrow H_2$) is maximally violating. Such points can be the minimum of the potential when $\kappa = 0$, where an axial U(1) symmetry, which is the one used to eliminate the term in Eq. (14), is enhanced. For $r = 0$ or $r \to \infty$, which means $v_2 = 0$ or $v_1 = 0$, the U(1) symmetry remains unbroken, and thus there is no massless

[2] h_i's are proportional to 2 by 2 unit matrices though we do not write them explicitly.

[3] A brief discussion is given in Appendix A.

Nambu-Goldstone boson in the spectrum. This vacuum realizes the Standard Model limit of the model, where there is no mixing between W/Z and W'/Z', and H_3 is the only source of the electroweak symmetry breaking ($v_3 = v$). When a small κ parameter is turned on, one can naturally realize $r \ll 1$ or $r \gg 1$. Since such parameter regions are close to the Standard Model limit, the constraints from the electroweak precision tests are not very severe. However, as we will see later, the searches for W'/Z' at the LHC experiments become important in such parameter regions.

The parameter r is related to the custodial symmetry: the symmetry between $W(W')$ and $Z(Z')$. The custodial symmetry becomes a good symmetry for a small r. This can be understood by the nature of W' and Z'. For $r \ll 1$, both W' and Z' mainly originate from $\mathrm{SU}(2)_1$, whereas for $r \gg 1$, Z' has a large $\mathrm{U}(1)_2$ fraction that W' does not have. We will explicitly see this feature, for example, in Sec. III B.

In general, demanding the vacuum in Eq. (15) as an extremum of the potential, we obtain the following relations:

$$\mu_1^2 = -\kappa\frac{v_2 v_3}{4v_1} - \frac{1}{2}(2v_1^2\lambda_1 + v_2^2\lambda_{12} + v_3^2\lambda_{31}), \tag{17}$$

$$\mu_2^2 = -\kappa\frac{v_3 v_1}{v_2} - \frac{1}{2}(v_1^2\lambda_{12} + 2v_2^2\lambda_2 + v_3^2\lambda_{23}), \tag{18}$$

$$\mu_3^2 = -\kappa\frac{v_1 v_2}{4v_3} - \frac{1}{2}(v_1^2\lambda_{31} + v_2^2\lambda_{23} + 2v_3^2\lambda_3). \tag{19}$$

For the stability of the potential at a large value of the Higgs fields, the following relations should be satisfied:

$$\lambda_1 > 0, \qquad \lambda_2 > 0, \qquad \lambda_3 > 0. \tag{20}$$

We will also see that

$$\kappa < 0 \tag{21}$$

is required from the local stability when $v_1, v_2, v_3 \neq 0$.

B. Higgs mass

From the Higgs potential, we can read off the following mass terms for the physical scalar particles.

1. Charged Higgs sector

The mass matrix of the charged Higgs fields is given by

$$V \supset \begin{pmatrix}\pi_1^+ & \pi_2^+ & \pi_3^+\end{pmatrix}\mathcal{M}_{\mathrm{CS}}^2\begin{pmatrix}\pi_1^- \\ \pi_2^- \\ \pi_3^-\end{pmatrix} = \begin{pmatrix}\pi_{W^+} & \pi_{W'^+} & H^+\end{pmatrix}\begin{pmatrix}0 & 0 & 0 \\ 0 & 0 & 0 \\ 0 & 0 & m_{H^\pm}^2\end{pmatrix}\begin{pmatrix}\pi_{W^-} \\ \pi_{W'^-} \\ H^-\end{pmatrix}, \tag{22}$$

where

$$\mathcal{M}_{\mathrm{CS}}^2 = \begin{pmatrix} -\frac{v_2 v_3}{2v_1}\kappa & -\frac{v_3}{2}\kappa & \frac{v_2}{2}\kappa \\ -\frac{v_3}{2}\kappa & -\frac{v_1 v_3}{2v_2}\kappa & \frac{v_1}{2}\kappa \\ \frac{v_2}{2}\kappa & \frac{v_1}{2}\kappa & -\frac{v_1 v_2}{2v_3}\kappa \end{pmatrix}, \tag{23}$$

$$m_{H^\pm}^2 = -2\frac{\kappa}{v_3}\frac{1+r^2}{r}v^2. \tag{24}$$

The fields $\pi_{W^\pm}$ and $\pi_{W'^\pm}$ are would-be Nambu-Goldstone (NG) bosons that are eaten by W and W', respectively. The relation between mass eigenstates and gauge eigenstates are

$$H^\pm = w_A^1\pi_1^\pm + w_A^2\pi_2^\pm + w_A^3\pi_3^\pm, \tag{25}$$

where

$$w_A^1 = \frac{1}{\sqrt{\frac{1}{v_1^2}+\frac{1}{v_2^2}+\frac{1}{v_3^2}}}\frac{1}{v_1} = \frac{r}{\sqrt{1+r^2}}\frac{v_3}{v}, \tag{26}$$

$$w_A^2 = \frac{1}{\sqrt{\frac{1}{v_1^2}+\frac{1}{v_2^2}+\frac{1}{v_3^2}}}\frac{1}{v_2} = \frac{1}{\sqrt{1+r^2}}\frac{v_3}{v}, \tag{27}$$

$$w_A^3 = -\frac{1}{\sqrt{\frac{1}{v_1^2}+\frac{1}{v_2^2}+\frac{1}{v_3^2}}}\frac{1}{v_3} = -\sqrt{1-\frac{v_3^2}{v^2}}. \tag{28}$$

2. Neutral CP-odd Higgs sector

The mass matrix for the CP-odd scalar fields is given by

$$V \supset \frac{1}{2}\begin{pmatrix}\pi_1^3 & \pi_2^3 & \pi_3^3\end{pmatrix}\mathcal{M}_{\mathrm{NS}}^2\begin{pmatrix}\pi_1^3 \\ \pi_2^3 \\ \pi_3^3\end{pmatrix} = \begin{pmatrix}\pi_Z & \pi_{Z'} & A^0\end{pmatrix}\begin{pmatrix}0 & 0 & 0 \\ 0 & 0 & 0 \\ 0 & 0 & m_{A^0}^2\end{pmatrix}\begin{pmatrix}\pi_Z \\ \pi_{Z'} \\ A^0\end{pmatrix}, \tag{29}$$

where

$$\mathcal{M}_{\mathrm{NS}}^2 = \mathcal{M}_{\mathrm{CS}}^2, \tag{30}$$

$$m_{A^0}^2 = m_{H^\pm}^2. \tag{31}$$

The physical CP-odd Higgs boson has the same mass as the charged Higgs boson given in Eq. (24). The fields π_Z and $\pi_{Z'}$ are would-be NG bosons that are eaten by Z and Z', respectively. The relation between mass eigenstates and gauge eigenstates are

$$A^0 = w_A^1\pi_1^3 + w_A^2\pi_2^3 + w_A^3\pi_3^3, \tag{32}$$

where w_A^1, w_A^2, and w_A^3 are given in Eqs. (26)–(28).

3. Neutral CP-even Higgs sector

The mass matrix for the neutral CP-even Higgs bosons is

$$V \supset \frac{1}{2}\begin{pmatrix} h_1 & h_2 & h_3 \end{pmatrix}\mathcal{M}^2_{\rm H}\begin{pmatrix} h_1 \\ h_2 \\ h_3 \end{pmatrix} = \begin{pmatrix} H & H' & h \end{pmatrix}\begin{pmatrix} m_H^2 & 0 & 0 \\ 0 & m_{H'}^2 & 0 \\ 0 & 0 & m_h^2 \end{pmatrix}\begin{pmatrix} H \\ H' \\ h \end{pmatrix}, \tag{33}$$

where

$$\mathcal{M}^2_{\rm H} = \begin{pmatrix} -\frac{v_2 v_3}{2v_1}\kappa + 4v_1^2\lambda_1 & \frac{v_3}{2}\kappa + 2v_1 v_2\lambda_{12} & \frac{v_2}{2}\kappa + 2v_1 v_3\lambda_{31} \\ \frac{v_3}{2}\kappa + 2v_1 v_2\lambda_{12} & -\frac{v_1 v_3}{2v_2}\kappa + 4v_2^2\lambda_2 & \frac{v_1}{2}\kappa + 2v_2 v_3\lambda_{23} \\ \frac{v_1}{2}\kappa + 2v_2 v_3\lambda_{23} & \frac{v_1}{2}\kappa + 2v_2 v_3\lambda_{23} & -\frac{v_1 v_2}{2v_3}\kappa + 4v_3^2\lambda_3 \end{pmatrix}. \tag{34}$$

The relations between mass eigenstates and gauge eigenstates are

$$\begin{pmatrix} H \\ H' \\ h \end{pmatrix} = \begin{pmatrix} w_H^1 & w_H^2 & w_H^3 \\ w_{H'}^1 & w_{H'}^2 & w_{H'}^3 \\ w_h^1 & w_h^2 & w_h^3 \end{pmatrix}\begin{pmatrix} h_1 \\ h_2 \\ h_3 \end{pmatrix}, \qquad \begin{pmatrix} h_1 \\ h_2 \\ h_3 \end{pmatrix} = \begin{pmatrix} w_H^1 & w_{H'}^1 & w_h^1 \\ w_H^2 & w_{H'}^2 & w_h^2 \\ w_H^3 & w_{H'}^3 & w_h^3 \end{pmatrix}\begin{pmatrix} H \\ H' \\ h \end{pmatrix}. \tag{35}$$

We define h as the lightest one, and thus $m_h = 125$ GeV. Note that $|w_h^i|^2$ is the h component in H_i. Since we assume H_3 is elementary and H_1 and H_2 are composite, $|w_h^3| = 1$ means h is completely elementary. If h is completely composite and arises from the dynamical sector, then $|w_h^3| = 0$. Our focus is partially composite h, i.e.,

$$|w_h^3| \neq 1, \qquad |w_h^3|^2 \gg |w_h^1|^2, \qquad |w_h^3|^2 \gg |w_h^2|^2. \tag{36}$$

C. Gauge sector

The mass terms of the gauge bosons are

$$\mathcal{L} \supset \begin{pmatrix} W_{0\mu}^+ & W_{1\mu}^+ \end{pmatrix}\mathcal{M}^2_{\rm CG}\begin{pmatrix} W_0^{-\mu} \\ W_1^{-\mu} \end{pmatrix} + \frac{1}{2}\begin{pmatrix} W_{0\mu}^3 & W_{1\mu}^3 & B_\mu \end{pmatrix}\mathcal{M}^2_{\rm NG}\begin{pmatrix} W_0^{3\mu} \\ W_1^{3\mu} \\ B^3 \end{pmatrix}, \tag{37}$$

where

$$\mathcal{M}^2_{\rm CG} = \frac{1}{4}\begin{pmatrix} g_0^2(v_1^2 + v_3^2) & -g_0 g_1 v_1^2 \\ -g_0 g_1 v_1^2 & g_1^2(v_2^2 + v_3^2) \end{pmatrix}, \tag{38}$$

$$\mathcal{M}^2_{\rm NG} = \frac{1}{4}\begin{pmatrix} g_0^2(v_1^2 + v_3^2) & -g_0 g_1 v_1^2 & -g_0 g_2 v_3^2 \\ -g_0 g_1 v_1^2 & g_1^2(v_2^2 + v_3^2) & -g_1 g_2 v_3^2 \\ -g_0 g_2 v_3^2 & -g_1 g_2 v_3^2 & g_2^2(v_2^2 + v_3^2) \end{pmatrix}. \tag{39}$$

The gauge boson masses are the eigenvalues of these mass matrices. In the $g_1 \gg g_{0,2}$ region, we find

$$m_W^2 \simeq \frac{1}{4}g_0^2 v^2\left(1 - \frac{g_0^2}{g_1^2}\frac{1}{(1+r^2)^2}\right), \tag{40}$$

$$m_{W'}^2 \simeq \frac{1}{4}g_1^2(v_1^2 + v_2^2)\left(1 + \frac{g_0^2}{g_1^2}\frac{1}{(1+r^2)^2}\right), \tag{41}$$

$$m_\gamma^2 = 0, \tag{42}$$

$$m_Z^2 \simeq \frac{1}{4}(g_0^2 + g_2^2)v^2\left(1 - \frac{(g_0^2 - g_2^2 r^2)^2}{g_1^2(g_0^2 + g_2^2)}\frac{1}{(1+r^2)^2}\right), \tag{43}$$

$$m_{Z'}^2 \simeq \frac{1}{4}g_1^2(v_1^2 + v_2^2)\left(1 + \frac{g_0^2 + g_2^2 r^4}{g_1^2}\frac{1}{(1+r^2)^2}\right). \tag{44}$$

The relation between mass eigenstates and gauge eigenstates are

$$\begin{pmatrix} W_\mu^\pm \\ W_\mu'^\pm \end{pmatrix} = \begin{pmatrix} w_W^0 & w_W^1 \\ w_{W'}^0 & w_{W'}^1 \end{pmatrix}\begin{pmatrix} W_{0\mu}^\pm \\ W_{1\mu}^\pm \end{pmatrix}, \qquad \begin{pmatrix} W_{0\mu}^\pm \\ W_{1\mu}^\pm \end{pmatrix} = \begin{pmatrix} w_W^0 & w_{W'}^0 \\ w_W^1 & w_{W'}^1 \end{pmatrix}\begin{pmatrix} W_\mu^\pm \\ W_\mu'^\pm \end{pmatrix}, \tag{45}$$

$$\begin{pmatrix} Z_\mu \\ Z'_\mu \\ A_\mu \end{pmatrix} = \begin{pmatrix} w_Z^0 & w_Z^1 & w_Z^2 \\ w_{Z'}^0 & w_{Z'}^1 & w_{Z'}^2 \\ w_A^0 & w_A^1 & w_A^2 \end{pmatrix}\begin{pmatrix} W_{0\mu}^3 \\ W_{1\mu}^3 \\ B_\mu \end{pmatrix}, \qquad \begin{pmatrix} W_{0\mu}^3 \\ W_{1\mu}^3 \\ B_\mu \end{pmatrix} = \begin{pmatrix} w_Z^0 & w_{Z'}^0 & w_A^0 \\ w_Z^1 & w_{Z'}^1 & w_A^1 \\ w_Z^2 & w_{Z'}^2 & w_A^2 \end{pmatrix}\begin{pmatrix} Z_\mu \\ Z'_\mu \\ A_\mu \end{pmatrix}. \tag{46}$$

We can find the expressions of w_X^i by diagonalizing the mass matrices.

We find some relations among parameters. A naive relation among m_W and $m_{W'}$ is $m_{W'}^2 - m_W^2 > 0$. But there is actually a more stringent bound:

$$m_{W'}^2 - m_W^2 \geq \frac{2m_W m_{W'}}{r}\sqrt{1-\frac{v_3^2}{v^2}}. \tag{47}$$

We can use this relation to find the lower bound on r,

$$r \geq \frac{2m_W m_{W'}}{m_{W'}^2 - m_W^2}\sqrt{1-\frac{v_3^2}{v^2}}. \tag{48}$$

We find another relation,

$$g_1 < \frac{m_{W'}}{\sqrt{v^2 - v_3^2}}. \tag{49}$$

We derive Eqs. (47) and (49) in Appendix C.

D. Couplings

In this section, we calculate the coupling constants between mass eigenstates. Since many of their expressions are complicated, we use the approximations that are valid when $g_1 \gg g_0$. We do not use this approximation in the numerical calculations performed later.

1. h-f-f couplings

The h couplings to the fermions and the fermion masses are given as

$$g_{ffh} = y_f \frac{w_h^3}{2}, \qquad m_f = y_f \frac{v_3}{2}. \tag{50}$$

From these formulas, we see that Yukawa couplings are always (v/v_3) times as large as their SM values. Since $v_3 < v \sim 246$ GeV as we can see from Eq. (16), the Yukawa coupling constants are always larger than their SM values. In order for the top Yukawa coupling to be small enough for perturbative calculations, too small v_3 is not allowed. For example, if we impose $y_t < 3y_t^{\rm SM}$, then the lower bound on v_3 is $\sim$80 GeV.

We introduce κ_f as the ratio of this coupling to the one in the SM,

$$\kappa_f \equiv \frac{g_{ffh}}{m_f/v} = \frac{v}{v_3} w_h^3. \tag{51}$$

Since $v_3 < v$, or the Yukawa couplings are larger than their SM values, this ratio is larger than one when $w_h^3 > v_3/v$. This leads the enhancement of $\mathrm{Br}(h \to ff)$. We do not consider extremely small values of w_h^3 [see Eq. (36)]. The choice is phenomenologically favored since the signal strengths around 125 GeV in both ATLAS and CMS look consistent with the SM Higgs boson.

2. V-f-f couplings

The gauge boson to fermion couplings are given by

$$g_{Zff} \simeq \frac{e}{s_Z c_Z}\left(T^3 - s_Z^2\left(1 + \frac{m_W^2}{m_{W'}^2}\frac{1}{1-2s_Z^2}\left(1-\frac{v_3^2}{v^2}\right)\right)Q\right), \tag{52}$$

$$g_{Z'ff} \simeq -\frac{e}{s_Z}\frac{m_W}{m_{W'}}\frac{1}{r}\sqrt{1-\frac{v_3^2}{v^2}}\left(\left(1 - r^2\frac{s_Z^2}{c_Z^2}\right)T^3 + r^2\frac{s_Z^2}{c_Z^2}Q\right), \tag{53}$$

$$g_{Wff} \simeq \frac{e}{s_Z}\left(1 - \frac{m_W^2}{m_{W'}^2}\frac{s_Z^2}{1-2s_Z^2}\left(1-\frac{v_3^2}{v^2}\right)\right), \tag{54}$$

$$g_{W'ff} \simeq -\frac{e}{s_Z}\frac{m_W}{m_{W'}}\frac{1}{r}\sqrt{1-\frac{v_3^2}{v^2}}, \tag{55}$$

where

$$\frac{1}{e^2} \equiv \frac{1}{g_0^2} + \frac{1}{g_1^2} + \frac{1}{g_2^2}, \tag{56}$$

and where s_Z and c_Z are defined through

$$s_Z^2 c_Z^2 \equiv \frac{e^2}{4\sqrt{2}G_F m_Z^2}. \tag{57}$$

3. h-V-V couplings

The Higgs boson couplings to the gauge bosons are given as follows:

$$\begin{aligned}\kappa_W &\equiv \frac{g_{WWh}}{2m_W^2/v} \\ &\simeq + \frac{r}{(1+r^2)^{3/2}}\sqrt{1-\frac{v_3^2}{v^2}}\left(r^2 - 2\frac{m_W^2}{m_{W'}^2}\right)w_h^1 \\ &\quad + \frac{1}{(1+r^2)^{3/2}}\sqrt{1-\frac{v_3^2}{v^2}}\left(1 + 2\frac{m_W^2}{m_{W'}^2}\right)w_h^2 + \frac{v_3}{v}w_h^3,\end{aligned} \tag{58}$$

$$\begin{aligned}\kappa_{W'} &\equiv \frac{g_{W'W'h}}{2m_{W'}^2/v} \\ &\simeq + \frac{r}{(1+r^2)^{3/2}}\frac{1}{\sqrt{1-\frac{v_3^2}{v^2}}}\left(1 + 2\frac{m_W^2}{m_{W'}^2}\left(1-\frac{v_3^2}{v^2}\right)\right)w_h^1 \\ &\quad + \frac{1}{(1+r^2)^{3/2}}\frac{1}{\sqrt{1-\frac{v_3^2}{v^2}}}\left(r^2 - 2\frac{m_W^2}{m_{W'}^2}\left(1-\frac{v_3^2}{v^2}\right)\right)w_h^2.\end{aligned} \tag{59}$$

Here we ignored $\mathcal{O}(m_W^4/m_{W'}^4)$ terms. Note that the h_3 component in h, w_h^3, does not contribute to $g_{W'W'h}$, namely h_3 does not couple to $W'W'$, at this order.

To see their qualitative feature, let us consider the case with $w_h^1 \sim w_h^2 \sim 0$ and $w_h^3 \sim 1$, namely the situation where the Higgs boson is almost elementary. In this case, we see that $\kappa_W \sim v_3/v \leq 1$, and $\mathrm{Br}(h \to WW)$ tends to be smaller than the SM prediction. In addition, we find $\kappa_{W'} \sim 0$ in that case, so the W'-loop effect on the $h \to \gamma\gamma$ process tends to be small due to the small fractions of w_h^1 and w_h^2. We can introduce κ_Z and $\kappa_{Z'}$ in a similar manner.

$$\kappa_Z \equiv \frac{g_{ZZh}}{2m_Z^2/v}$$
$$\simeq + \frac{r}{(1+r^2)^{3/2}}\sqrt{1-\frac{v_3^2}{v^2}}\left(r^2 - 2\frac{m_W^2}{m_{W'}^2}\left(1 - r^2\frac{s_Z^2}{c_Z^2}\right)\right)w_h^1$$
$$+ \frac{1}{(1+r^2)^{3/2}}\sqrt{1-\frac{v_3^2}{v^2}}\left(1 + 2\frac{m_W^2}{m_{W'}^2}\left(1 - r^2\frac{s_Z^2}{c_Z^2}\right)\right)w_h^2$$
$$+ \frac{v_3}{v}w_h^3, \tag{60}$$

$$\kappa_{Z'} \equiv \frac{g_{Z'Z'h}}{2m_{Z'}^2/v}$$
$$\simeq + \frac{r}{(1+r^2)^{3/2}}\frac{1}{\sqrt{1-\frac{v_3^2}{v^2}}}\left(1 + 2\frac{m_W^2}{m_{W'}^2}\left(1 - \frac{v_3^2}{v^2}\right)\right.$$
$$\left.\times\left(1 - r^2\frac{s_Z^2}{c_Z^2}\right)\right)w_h^1$$
$$+ \frac{1}{(1+r^2)^{3/2}}\frac{1}{\sqrt{1-\frac{v_3^2}{v^2}}}\left(r^2 - 2\frac{m_W^2}{m_{W'}^2}\left(1 - \frac{v_3^2}{v^2}\right)\right.$$
$$\left.\times\left(1 - r^2\frac{s_Z^2}{c_Z^2}\right)\right)w_h^2. \tag{61}$$

The $g_{VV'h}$ couplings are also calculated to be

$$\frac{g_{WW'h}}{2m_W m_{W'}/v} \simeq -\frac{1}{(1+r^2)^{3/2}}\left(r^2 - \frac{m_W^2}{m_{W'}^2}\left((1-r^2) + r^2\frac{v_3^2}{v^2}\right)\right)w_h^1$$
$$+ \frac{1}{r(1+r^2)^{3/2}}\left(r^2 - \frac{m_W^2}{m_{W'}^2}\left((1-r^2) - \frac{v_3^2}{v^2}\right)\right)w_h^2$$
$$- \frac{m_W^2}{m_{W'}^2}\frac{v_3}{v}\frac{1}{r}\sqrt{1-\frac{v_3^2}{v^2}}w_h^3, \tag{62}$$

$$\frac{g_{ZZ'h}}{2m_Z m_{Z'}/v} \simeq -\frac{1}{(1+r^2)^{3/2}}\left(r^2 - \frac{m_W^2}{m_{W'}^2}\left((1-r^2) + r^2\frac{v_3^2}{v^2}\right)\right.$$
$$\left.\times\left(1 - r^2\frac{s_Z^2}{c_Z^2}\right)\right)w_h^1 + \frac{1}{r(1+r^2)^{3/2}}$$
$$\times\left(r^2 - \frac{m_W^2}{m_{W'}^2}\left((1-r^2) - \frac{v_3^2}{v^2}\right)\right.$$
$$\left.\times\left(1 - r^2\frac{s_Z^2}{c_Z^2}\right)\right)w_h^2 - \frac{m_W^2}{m_{W'}^2}\frac{v_3}{v}\frac{1}{r}\sqrt{1-\frac{v_3^2}{v^2}}$$
$$\times\left(1 - r^2\frac{s_Z^2}{c_Z^2}\right)w_h^3. \tag{63}$$

From these expressions, we see that the difference between $W(W')$ and $Z(Z')$ becomes larger (smaller) when $r > 1$ ($r < 1$).

4. h-H^--H^+ couplings

The coupling between the Higgs boson and the charged Higgs bosons are

$$\mathcal{L} \supset -g_{H^-H^+h}H^+H^-h, \tag{64}$$

where

$$g_{H^-H^+h} \simeq + \frac{m_{H^\pm}^2}{v}\frac{v_3^2}{v^2}\left(\sqrt{1-\frac{v_3^2}{v^2}}\frac{r}{(1+r^2)^{3/2}}w_h^1\right.$$
$$\left. + \sqrt{1-\frac{v_3^2}{v^2}}\frac{1}{(1+r^2)^{3/2}}w_h^2 + \frac{v_3}{v}\frac{r^2}{(1+r^2)^2}w_h^3\right). \tag{65}$$

Here we assume $m_{H^\pm}^2 \gg v^2, v_3^2$. We define $\kappa_{H^\pm}$ as follows:

$$\kappa_{H^\pm} \equiv \frac{g_{H^-H^+h}}{2m_{H^\pm}^2/v}. \tag{66}$$

5. WWZ, $WW'Z$, and WWZ' couplings

Finally, the triple gauge boson vertices are given by

$$g_{WWZ} \simeq \frac{e}{s_Z}c_Z\left(1 - \frac{m_W^2}{m_{W'}^2}\frac{1}{(1+r^2)(1-2s_Z^2)}\right.$$
$$\left.\times\left(1 + r^2\frac{s_Z^2}{c_Z^2}\right)\left(1 - \frac{v_3^2}{v^2}\right)\right), \tag{67}$$

$$g_{WW'Z} \simeq -\frac{e}{s_Z}c_Z\frac{m_W}{m_{W'}}\frac{r}{(1+r^2)(1-s_Z^2)}\sqrt{1-\frac{v_3^2}{v^2}}, \tag{68}$$

$$g_{WWZ'} \simeq -\frac{e}{s_Z}c_Z\frac{m_W}{m_{W'}}\frac{r}{(1+r^2)(1-s_Z^2)}\sqrt{1-\frac{v_3^2}{v^2}}\sqrt{1-s_Z^2}. \tag{69}$$

We find the VVV' couplings are suppressed by $(m_W/m_{W'})$ compared to the WWZ coupling.

III. CONSTRAINTS ON W' AND Z'

A. Constraints from electroweak precision measurements

In this section, we discuss the electroweak constraints. Because of the existence of the extra gauge bosons, W' and Z', the parameters such as $\hat{S}$ are nonzero at tree level and give a severe constraint on the model because these parameters are measured to be at most as small as of order the one-loop level.

To calculate the electroweak parameters, $\hat{S}$, $\hat{T}$, $\hat{U}$, W, and Y (see Ref. [40] for definitions), we calculate the quadratic terms of gauge bosons in the momentum-space effective action. They are written as

$$-\frac{1}{2}g_{\mu\nu}\begin{pmatrix} W_0^\mu & B^\mu & W_1^\mu \end{pmatrix}\begin{pmatrix} \Pi_{00} & \Pi_{02} & \Pi_{01} \\ \Pi_{20} & \Pi_{22} & \Pi_{21} \\ \Pi_{10} & \Pi_{12} & \Pi_{11} \end{pmatrix}\begin{pmatrix} W_0^\nu \\ B^\nu \\ W_1^\nu \end{pmatrix} + (q_\mu q_\nu \text{ terms}), \tag{70}$$

where

$$\Pi_{00} = \frac{1}{g_0^2}q^2 - \frac{1}{4}(v_1^2 + v_3^2), \tag{71}$$

$$\Pi_{22} = \frac{1}{g_2^2}q^2 - \frac{1}{4}(v_2^2 + v_3^2), \tag{72}$$

$$\Pi_{11} = \frac{1}{g_1^2}q^2 - \frac{1}{4}(v_1^2 + v_2^2), \tag{73}$$

$$\Pi_{01} = \frac{1}{4}v_1^2, \tag{74}$$

$$\Pi_{02} = \frac{1}{4}v_3^2, \tag{75}$$

$$\Pi_{12} = \frac{1}{4}v_2^2, \tag{76}$$

and $\Pi_{xy} = \Pi_{yx}$. We consider only $g_{\mu\nu}$ terms. Since W_1 is decoupled from the fermion sector, we integrate it out. Then the quadratic terms become

$$-\frac{1}{2}g_{\mu\nu}\begin{pmatrix} W_0^\mu & B^\mu \end{pmatrix}\begin{pmatrix} \Pi_{W_3W_3} & \Pi_{W_3B} \\ \Pi_{W_3B} & \Pi_{BB} \end{pmatrix}\begin{pmatrix} W_0^\nu \\ B^\nu \end{pmatrix}, \tag{77}$$

where

$$\Pi_{W_3W_3} = \Pi_{00} - \Pi_{01}(\Pi_{11})^{-1}\Pi_{10}, \tag{78}$$

$$\Pi_{W_3B} = \Pi_{02} - \Pi_{01}(\Pi_{11})^{-1}\Pi_{12}, \tag{79}$$

$$\Pi_{BB} = \Pi_{22} - \Pi_{21}(\Pi_{11})^{-1}\Pi_{12}. \tag{80}$$

Their explicit expressions are given in Appendix B. In a similar manner, we can calculate the charged sector, and we find $\Pi_{W_1W_1}(q^2) = \Pi_{W_3W_3}(q^2)$. Therefore $\hat{T} = \hat{U} = 0$ in this model. Using the definition given in Ref. [40], we find

$$\hat{S} = \frac{g_0^2 v_1^2 v_2^2}{g_1^2(v_1^2 + v_2^2)^2 + g_0^2 v_1^4}, \tag{81}$$

$$\hat{T} = 0, \tag{82}$$

$$\hat{U} = 0, \tag{83}$$

$$W = 4m_W^2\frac{g_0^2}{g_1^2}\frac{1}{v_1^2 + v_2^2}\frac{v_1^4}{g_1^2(v_1^2 + v_2^2)^2 + g_0^2 v_1^4}, \tag{84}$$

$$Y = 4m_W^2\frac{g_2^2}{g_1^2}\frac{1}{v_1^2 + v_2^2}\frac{v_2^4}{g_1^2(v_1^2 + v_2^2)^2 + g_2^2 v_2^4}. \tag{85}$$

The central values, standard deviations, and correlations of these parameters are given in Table 4 in Ref. [40].

$$10^3\hat{S} = 0 \pm 1.3 \equiv 10^3(\hat{S}_0 \pm \sigma_{\hat{S}}), \tag{86}$$

$$10^3\hat{T} = 0.1 \pm 0.9 \equiv 10^3(\hat{T}_0 \pm \sigma_{\hat{T}}), \tag{87}$$

$$10^3 Y = 0.1 \pm 1.2 \equiv 10^3(\hat{Y}_0 \pm \sigma_{\hat{Y}}), \tag{88}$$

$$10^3 W = -0.4 \pm 0.8 \equiv 10^3(\hat{W}_0 \pm \sigma_{\hat{W}}), \tag{89}$$

$$\rho = \begin{pmatrix} 1 & 0.68 & 0.65 & -0.12 \\ 0.68 & 1 & 0.11 & 0.19 \\ 0.65 & 0.11 & 1 & -0.59 \\ -0.12 & 0.19 & -0.59 & 1 \end{pmatrix}. \tag{90}$$

The confidence ellipse is given as

$$\vec{v}^T V^{-1}\vec{v} = \sigma_{\text{C.L.}}^2, \tag{91}$$

where

$$\vec{v}^T = 10^3\begin{pmatrix} \hat{S} - \hat{S}_0 & \hat{T} - \hat{T}_0 & Y - Y_0 & W - W_0 \end{pmatrix}, \tag{92}$$

$$V = (10^3)^2\begin{pmatrix} \sigma_{\hat{S}} & 0 & 0 & 0 \\ 0 & \sigma_{\hat{T}} & 0 & 0 \\ 0 & 0 & \sigma_Y & 0 \\ 0 & 0 & 0 & \sigma_W \end{pmatrix}\rho\begin{pmatrix} \sigma_{\hat{S}} & 0 & 0 & 0 \\ 0 & \sigma_{\hat{T}} & 0 & 0 \\ 0 & 0 & \sigma_Y & 0 \\ 0 & 0 & 0 & \sigma_W \end{pmatrix}, \tag{93}$$

and where

$$\sigma_{\text{CL}}^2 = \begin{cases} 4.71957 & (68.27\%\ \text{C.L.}) \\ 7.77944 & (90\%\ \text{C.L.}) \\ 9.48773 & (95\%\ \text{C.L.}) \\ 13.2767 & (99\%\ \text{C.L.}) \end{cases}. \tag{94}$$

The set of parameters should be in this ellipse.

There are three parameters relevant for the calculations, g_1, $r \equiv v_2/v_1$, and v_3. The rest of the parameters such as g_0, g_2, and v_1 (or v_2) are fixed so that α, M_Z, and G_F are correctly reproduced. Numerical results are shown in Figs. 2–4, where we take the mass of W', $M_{W'}$, as the horizontal axis. In Fig. 2, we show excluded parameter regions with fixed r, and those with fixed v_3 are shown in Figs. 3 and 4. The regions to the left of the red (light gray) lines are excluded from the electroweak precision tests. We see that the constraint from the electroweak precision measurements is almost independent of the values of g_1 and r but depend on v_3. The lower bound on $m_{W'}$ is typically 1 TeV (2 TeV) for $v_3 = 200$ GeV (100 GeV).

For $r = 1$, corresponding to the parity conserving model for the dynamical sector, one can see that the gauge coupling constant g_1 needs to be large such as $g_1 \sim 10$ in order to evade the electroweak constraints (see Fig. 2). With such a large value, the tree level analysis becomes not reliable.

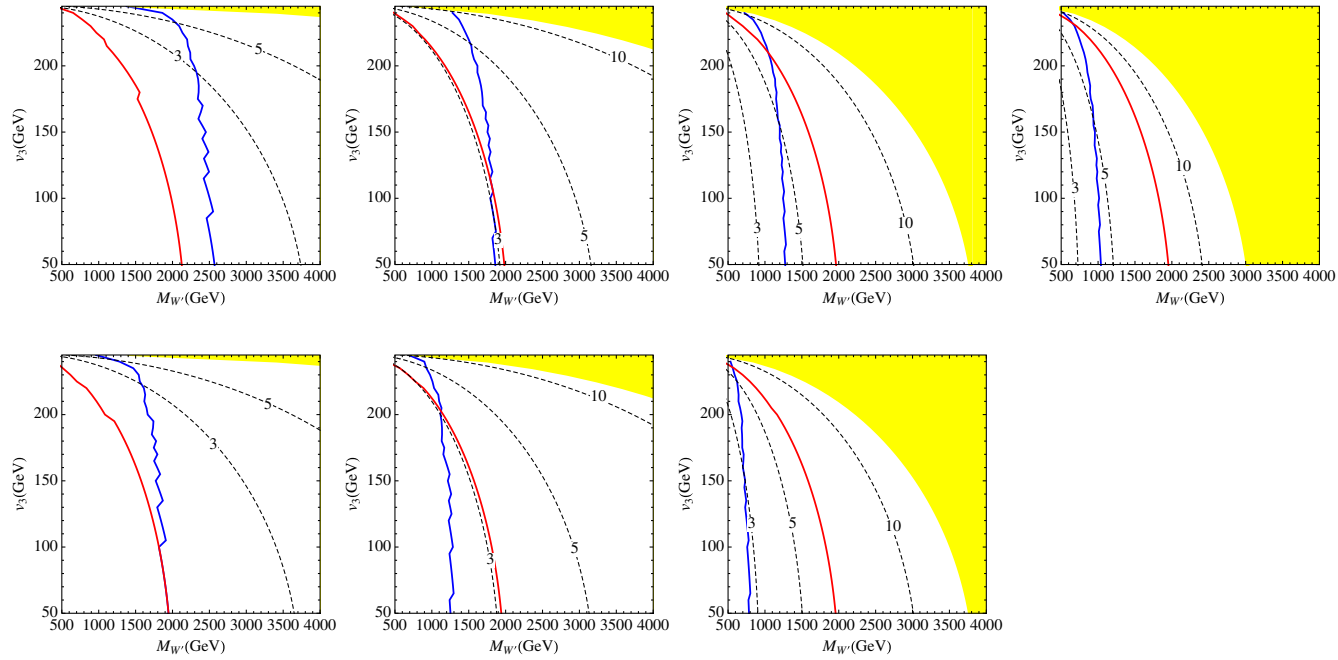

FIG. 2 (color online). Constraints in the $(m_{W'}, v_3)$ plane. The left side of the red and blue (light gray and dark gray) lines are excluded by the electroweak precision measurements and the W'/Z' search by the LHC, respectively. The numbers on the dashed lines are g_1 values. The yellow (shaded) region represents the region in which $g_1 \geq 4\pi$. In the first (second) row, we take $r = 0.1, 0.2, 0.5, 1$ (10, 5, 2) from the left to right columns.

On the other hand, for $r \ll 1$ or $r \gg 1$, there can be consistent parameter regions with g_1 much smaller than 4π (see Figs. 3 and 4). This suggests that the dynamical sector is either parity violating, such as chiral theories, or a theory that does not provide a particle picture for the vector resonances, unlike the QCD.

B. Constraints from direct searches for W' and Z' at the LHC

In this section, we discuss the bounds from the direct searches for W' and Z' bosons at the LHC experiments. Both ATLAS and CMS groups provide bounds on the combinations $\sigma \cdot \mathrm{Br}$ for each decay modes as a function of the mass of the W' and Z'. Since there are couplings to fermions through the mixing with Standard Model gauge bosons, W' and Z' can be produced via Drell-Yan processes. If the leptonic decay modes, namely $W' \to \ell\nu$ and $Z' \to \ell\ell$, have a sizable branching fraction, there are quite strong bounds. Whereas when W' is almost fermiophobic, its main decay mode is $W' \to WZ$. We, therefore, consider constraints from both processes: $pp \to W' \to WZ$, $pp \to W' \to \ell\nu$, and $pp \to Z' \to \ell\ell$.

We here give some qualitative discussion. The production cross sections are proportional to couplings squared,

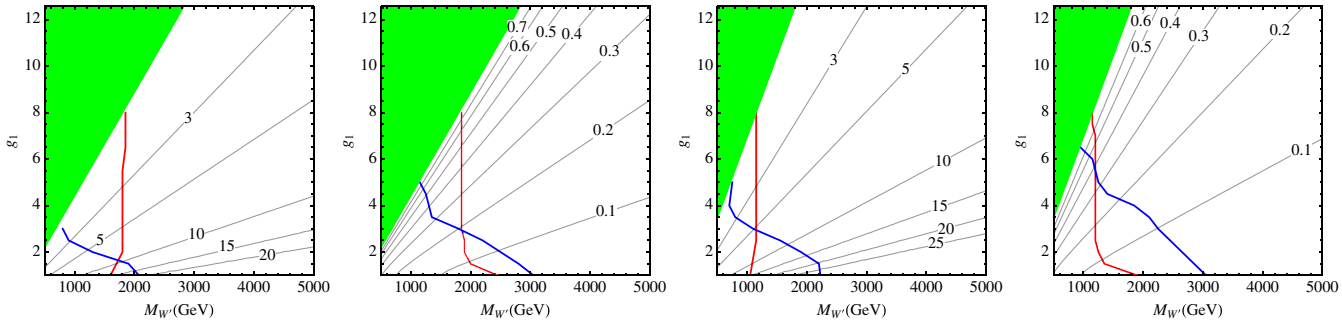

FIG. 3 (color online). Constraints in the $(m_{W'}, g_1)$ plane. No physical solutions are in the left side of the green (shaded region) line, namely the gauge couplings and/or VEV's become complex numbers there. The left side of the red and blue (light gray and dark gray) lines are excluded by the electroweak precision measurements and the W'/Z' search by the LHC, respectively. From the left to right panels we take $v_3 = 100$ GeV $(r > 1)$, $v_3 = 100$ GeV $(r < 1)$, $v_3 = 200$ GeV $(r > 1)$, and $v_3 = 200$ GeV $(r < 1)$.

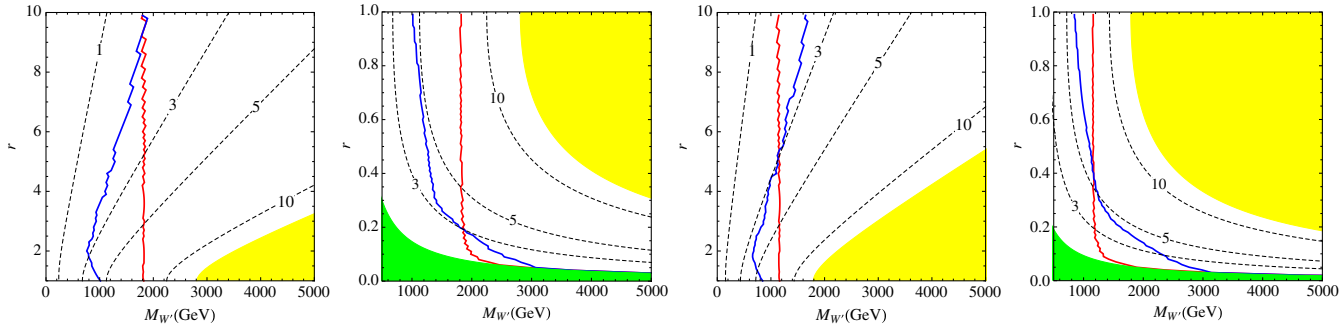

FIG. 4 (color online). Constraints in the $(m_{W'}, r)$ plane. No physical solutions are in the green (dark shaded) region, namely the gauge couplings and/or VEV's become complex numbers there. The left side of the red and blue (light gray and dark gray) lines are excluded by the electroweak precision measurements and the W'/Z' search by the LHC, respectively. From the left to right panels we take $v_3 = 100$ GeV $(r > 1)$, $v_3 = 100$ GeV $(r < 1)$, $v_3 = 200$ GeV $(r > 1)$, and $v_3 = 200$ GeV $(r < 1)$.

$$\sigma(q\bar{q} \to Z') \propto (g^2_{Z'ffL} + g^2_{Z'ffR}) \tag{95}$$

$$\simeq \frac{e^2}{s_Z^2}\frac{m_W^2}{m_{W'}^2}\frac{1}{r^2}\left(1-\frac{v_3^2}{v^2}\right)\left[\left(\left(1-r^2\frac{s_Z^2}{c_Z^2}\right)T^3 + r^2\frac{s_Z^2}{c_Z^2}Q\right)^2 + \left(r^2\frac{s_Z^2}{c_Z^2}Q\right)^2\right], \tag{96}$$

$$\sigma(q\bar{q}' \to W') \propto g^2_{W'ff} \tag{97}$$

$$\simeq \frac{e^2}{s_Z^2}\frac{m_W^2}{m_{W'}^2}\frac{1}{r^2}\left(1-\frac{v_3^2}{v^2}\right). \tag{98}$$

In the large r region, productions of W' are suppressed but Z' is enhanced. Hence Z', rather than W', is expected to give a stronger bound on parameter space in the large r region. On the other hand, both give similar bounds in the small r region. Notice that this difference between W' and Z' is due to large breaking of the custodial symmetry as we discussed in Sec. II. We show the cross sections of W' and Z' via Drell-Yan production at LHC in Fig. 5. The r dependence discussed here is now apparent in the left column in this figure.

The partial decay widths of W' and Z' are

$$\Gamma(Z' \to WW) \simeq \frac{1}{48\pi}\frac{m_{W'}^3}{v^2}\frac{r^2}{(1+r^2)^2}\left(1-\frac{v_3^2}{v^2}\right), \tag{99}$$

$$\Gamma(Z' \to Zh) \simeq \frac{1}{48\pi}\frac{m_{W'}^3}{v^2}\frac{r^2}{(1+r^2)^3}(-rw_h^1 + w_h^2)^2, \tag{100}$$

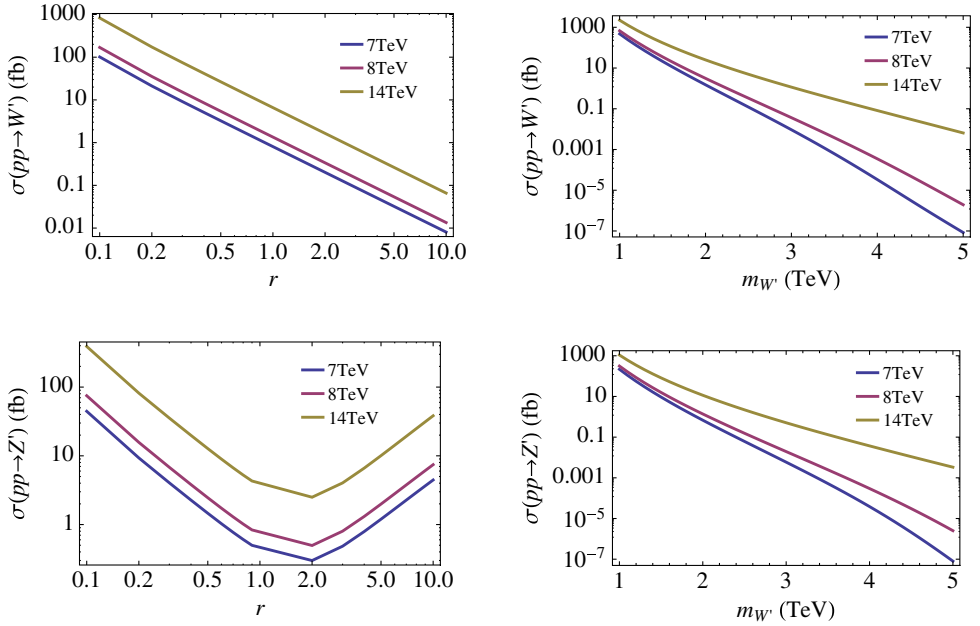

FIG. 5 (color online). The production cross section of W' and Z' via the Drell-Yan process as functions of r and $m_{W'}$. We take $m'_W = 1500$ GeV and $v_3 = 200$ GeV in the left column, and $v_3 = 200$ GeV and $r = 0.2$ in the right column. Here $\sigma(pp \to W') = \sigma(pp \to W'^-) + \sigma(pp \to W'^+)$. Here we use CTEQ6 for PDFs [47].

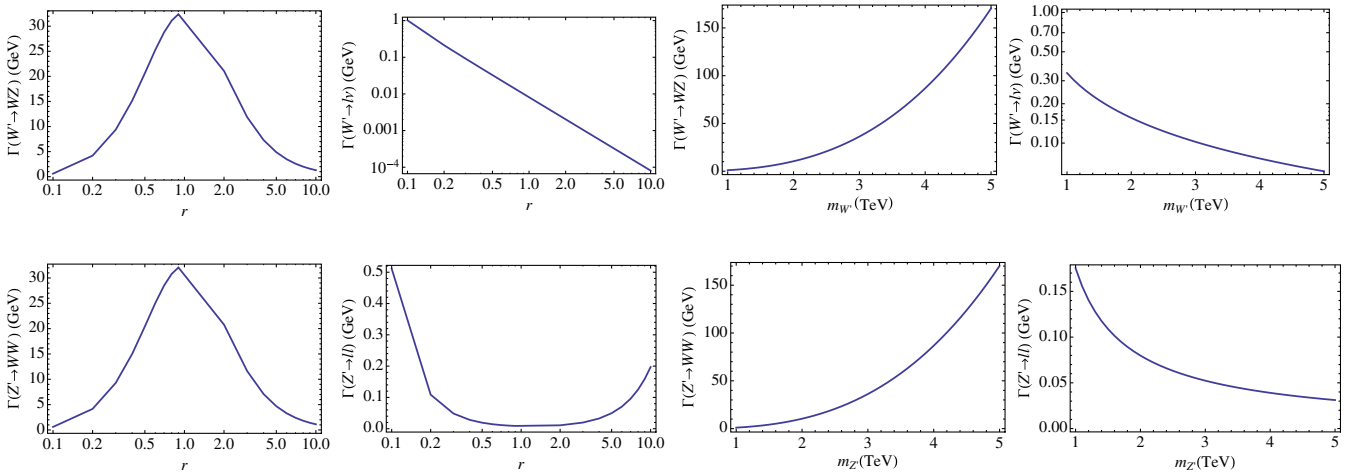

FIG. 6 (color online). The partial decay widths of W' and Z' as functions of r and $m_{W'}$. We take $m_{W'} = 1500$ GeV and $v_3 = 200$ GeV in the left four panels, and $v_3 = 200$ GeV and $r = 0.2$ in the right four panels. Here $l\nu = e\nu + \mu\nu$, and $ll = ee + \mu\mu$.

$$\Gamma(Z' \to f\bar{f}') \simeq \frac{1}{24\pi} N_c \frac{m_W^2}{m_{W'}} \frac{e^2}{s_Z^2} \frac{1}{r^2} \left(1 - \frac{v_3^2}{v^2}\right) \left(\left(\left(1 - r^2 \frac{s_Z^2}{c_Z^2}\right) T^3 + r^2 \frac{s_Z^2}{c_Z^2} Q \right)^2 + \left(r^2 \frac{s_Z^2}{c_Z^2} Q \right)^2 \right), \tag{101}$$

$$\Gamma(W' \to WZ) \simeq \frac{1}{48\pi} \frac{m_{W'}^3}{v^2} \frac{r^2}{(1+r^2)^2} \left(1 - \frac{v_3^2}{v^2}\right), \tag{102}$$

$$\Gamma(W' \to Wh) \simeq \frac{1}{48\pi} \frac{m_{W'}^3}{v^2} \frac{r^2}{(1+r^2)^3} (-r w_h^1 + w_h^2)^2, \tag{103}$$

$$\Gamma(W' \to f\bar{f}') \simeq \frac{1}{48\pi} N_c \frac{m_W^2}{m_{W'}} \frac{e^2}{s_Z^2} \frac{1}{r^2} \left(1 - \frac{v_3^2}{v^2}\right). \tag{104}$$

Here we keep leading terms in the $(m_W/m_{W'})$ expansion. We find that $\Gamma(Z' \to WW) \simeq \Gamma(W' \to WZ)$ and $\Gamma(Z' \to Zh) \simeq \Gamma(W' \to Wh)$ in this approximation. To see which of bosonic and fermionic decay modes is more important, we take their ratio,

$$\frac{\Gamma(W' \to WZ)}{\Gamma(W' \to f\bar{f}')} \simeq \frac{1}{4N_c} \frac{m_{W'}^4}{m_W^4} \frac{r^4}{(1+r^2)^2}. \tag{105}$$

We see that the bosonic decay mode is dominant except for the small r region. The Z' case is similar to Eq. (105) in the small r region, but it has extra r^{-2} in the large r region. Then $Z' \to f\bar{f}'$ as well as $Z' \to WW$ is important in the large r region. We plot partial decay widths in Fig. 6. The qualitative features discussed here are explicit as one can see in this figure.

Now we calculate $\sigma \cdot \mathrm{Br}$ for W' and Z', and compare the results from the searches at the LHC. We use the bounds on $pp \to W' \to WZ$ [41,42], $pp \to W' \to \ell\nu$ [43,44], and $pp \to Z' \to \ell\ell$ [45,46]. In this section, we restrict ourselves to consider the parameter space in which Eq. (36) is satisfied. Then we can omit the $V' \to Vh$ process. We also omit some other channels including heavier Higgs bosons and/or charged scalars, which highly depend on parameters in the Higgs potential. After taking into account these processes, the constraints might be weaker because they change the total decay width.

The numerical results are shown in Figs. 2–4 as blue (dark gray) lines. In a large parameter space, the electroweak precision test gives a stronger bound. The exceptions are regions with large and small r, that is, where g_1 can be small. Since the W'/Z' to fermion couplings are induced by the gauge boson mixings of order g_0/g_1, the production and decay rates are enhanced for a small g_1. In these regions, the LHC experiments are starting to give stronger bounds than the electroweak precision tests (see Fig. 3).

IV. SIGNAL STRENGTH OF 125 GEV HIGGS

The lightest Higgs boson h is a mixture of H_1, H_2, and H_3, and thus the properties are modified from the Standard Model predictions. We here discuss the production/decay properties of h. We start off by calculating ratios of partial decay widths. In the processes that exist at tree level, they are given as the ratio of the corresponding couplings given in Sec. II D,

$$\frac{\Gamma(h \to ff)}{\Gamma(h \to ff)_{\mathrm{SM}}} = \kappa_f^2, \qquad \frac{\Gamma(h \to WW)}{\Gamma(h \to WW)_{\mathrm{SM}}} = \kappa_W^2, \qquad \frac{\Gamma(h \to ZZ)}{\Gamma(h \to ZZ)_{\mathrm{SM}}} = \kappa_Z^2. \tag{106}$$

We also define κ's for the loop induced processes,

$$\kappa_g^2 \equiv \frac{\Gamma(h \to gg)}{\Gamma(h \to gg)_{\mathrm{SM}}} = \frac{\sigma(gg \to h)}{\sigma(gg \to h)_{\mathrm{SM}}}, \tag{107}$$

$$\kappa_\gamma^2 \equiv \frac{\Gamma(h \to \gamma\gamma)}{\Gamma(h \to \gamma\gamma)_{\mathrm{SM}}}. \tag{108}$$

The diagrams that contribute to κ_g^2 are the same as those in the Standard Model. The only difference from the Standard

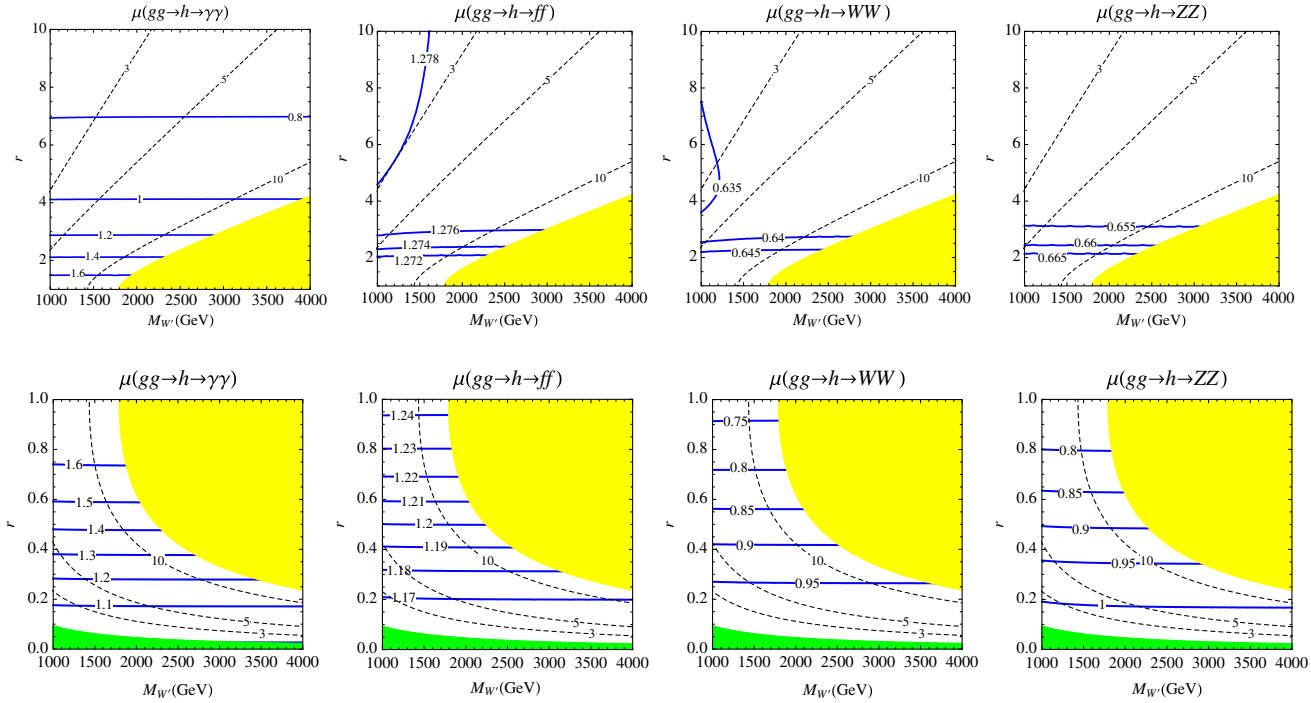

FIG. 7 (color online). Signal strengths on the $(M_{W'}, r)$ plane. The blue (dark gray) lines and dashed lines represent the signal strengths and g_1 values, respectively. The vertical axis is the ratio of the two VEVs, $r = v_2/v_1$. The yellow (light shaded) region stands for the region in which $g_1 > 4\pi$. In the green (dark shaded) region, the gauge couplings and/or VEV's become complex numbers. The upper (lower) column shows the $r > 1$ ($r < 1$) region. The parameter choices here are $w_h^1 = 0.1$, $w_h^2 = 0.5$, and $v_3 = 200$ GeV.

Model is the h couplings to the SM fermions that are given as κ_f. Hence

$$\kappa_g^2 = \kappa_f^2. \tag{109}$$

κ_γ is more complicated because W' and $H^\pm$ contribute to the process as well. The partial decay width for $h \to \gamma\gamma$ is given as

$$\Gamma(h \to \gamma\gamma) \simeq m_h^3 \frac{\alpha_{em}^2}{16\pi^3}\sqrt{2}G_F \left| \frac{1}{3}Q_t^2 N_c \kappa_f - 2.1\kappa_W - \frac{7}{4}\kappa_{W'} + \frac{1}{12}\kappa_{H^\pm} \right|^2. \tag{110}$$

Here we take $m_h \simeq 125$ GeV. Then we have

$$\kappa_\gamma^2 \simeq \left| \left(0.27\frac{v}{v_3} - 1.3\frac{v_3}{v}\right) w_h^3 + 0.005\kappa_{H^\pm} - 1.3\frac{1}{(1+r^2)^{3/2}}\sqrt{1-\frac{v_3^2}{v^2}}(r^3 w_h^1 + w_h^2) - 1.1\frac{r}{(1+r^2)^{3/2}}\frac{1}{\sqrt{1-\frac{v_3^2}{v^2}}}(w_h^1 + r w_h^2) \right|^2. \tag{111}$$

There are four terms in Eq. (111): The first term consists of a top quark contribution and a part of W contributions.

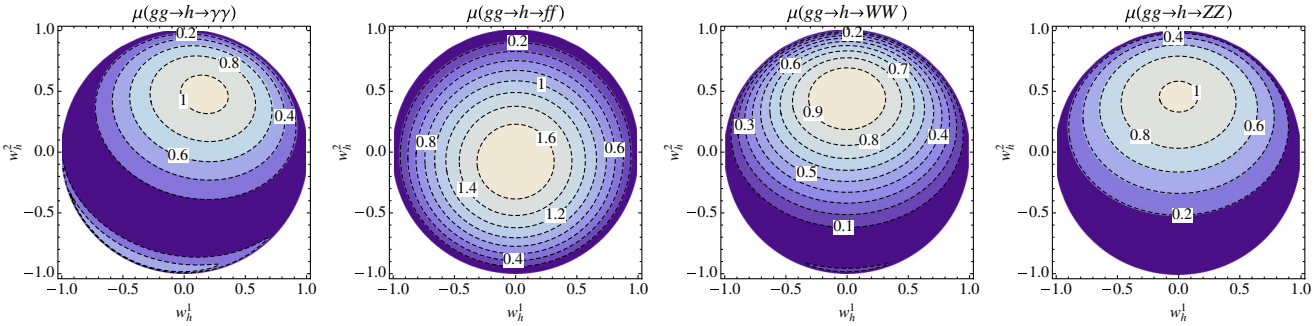

FIG. 8 (color online). Signal strengths on the (w_h^1, w_h^2) plane. The numbers on the dashed lines are the signal strengths. The parameter choices here are $v_3 = 200$ GeV, $m_{W'} = 2500$ GeV, and $r = 0.1$.

The second term is the charged scalar contribution. The third term is a part of W contributions. The fourth term is the W' contribution. We take v_3 as the same order as v to keep the perturbativity of the Yukawa coupling. Then we find that the charged scalar contribution is negligible. As long as we take the partially composite-ness condition in Eq. (36), the third term is negligible. On the other hand, the fourth term can be visible because its denominator becomes small for $v_3 \sim v$. Since the fourth term highly depends on r, the r dependence of κ_γ is large. We can calculate signal strengths by using κ's.

$$\mu(gg \to h \to X) = \frac{\kappa_g^2 \kappa_X^2}{\kappa_f^2 \mathrm{Br}^{\mathrm{SM}}_{h\to ff} + \kappa_W^2 \mathrm{Br}^{\mathrm{SM}}_{h\to WW} + \kappa_Z^2 \mathrm{Br}^{\mathrm{SM}}_{h\to ZZ} + \kappa_g^2 \mathrm{Br}^{\mathrm{SM}}_{h\to gg} + \kappa_\gamma^2 \mathrm{Br}^{\mathrm{SM}}_{h\to\gamma\gamma} + \kappa_{Z\gamma}^2 \mathrm{Br}^{\mathrm{SM}}_{h\to Z\gamma}} \tag{112}$$

$$\simeq \frac{\frac{v^2}{v_3^2}(w_h^3)^2}{\frac{3}{4}\frac{v^2}{v_3^2}(w_h^3)^2 + \frac{1}{4}\left(\frac{r^3}{(1+r^2)^{3/2}}\sqrt{1-\frac{v_3^2}{v^2}}w_h^1 + \frac{1}{(1+r^2)^{3/2}}\sqrt{1-\frac{v_3^2}{v^2}}w_h^2 + \frac{v_3}{v}w_h^3\right)^2}\kappa_X^2. \tag{113}$$

Here we calculate $\mathrm{Br}^{\mathrm{SM}}_{h\to X}$ with $m_h = 125$ GeV. Since we take $v_3 \sim v$ and $|w_h^3|^2 \gg |w_h^1|^2, |w_h^2|^2$, the r dependence is only in κ_X. Therefore, the r dependences of κ_γ, κ_f, and $\kappa_{W/Z}$ are large, absent, and weak, respectively. Another important feature is the $m_{W'}$ dependence. We find that the $m_{W'}$ dependence is absent at the leading order. These features are shown in Fig. 7. In this figure, we plot the signal strengths in the $(m_{W'}, r)$ plane with $w_h^1 = 0.1$, $w_h^2 = 0.5$. In this w_h^1 and w_h^2 choice, h is $\sim$30% composite because $|w_h^1|^2 + |w_h^2|^2 \simeq 0.3$. These calculations are performed numerically, and we do not use the approximated formulas given in this section.

We also show the signal strengths on the (w_h^1, w_h^2) plane. We take $v_3 = 200$ GeV, $m_{W'} = 2500$ GeV, and $r = 0.1$ in Fig. 8.[4] We find that the $w_h^1 \sim w_h^2 \sim 0$ region is disfavored. One of them, w_h^2 in this example, should take a sizable value. This means that the lightest Higgs boson has to have a component of not only the elementary sector (H_3) but also the composite sector (H_1 and H_2), namely the Higgs boson needs to be partially composite.

V. CONCLUSION

In this paper we constructed a model in which W/Z and the Higgs boson are partially composite, and we explore the effects of new particles on the electroweak precision measurements and the signal strength of the Higgs boson. We showed that the constraints on W' and Z' from the electroweak precision measurements and direct searches of them push their lower mass bounds a few TeV.

In the model we consider, one can take the decoupling limit where $v_1 = 0$ or $v_2 = 0$. In this limit, W'/Z' decouple from the Standard Model particles. The vacuum close to such points can naturally be realized since it is controlled by a soft breaking term of an axial U(1) symmetry, κ, in the potential. In such a vacuum, e.g., $r \equiv v_2/v_1 \gtrsim 5$ or $r \lesssim 0.2$, we find that a relatively small g_1, in which perturbative calculation is valid, is consistent with the electroweak precision tests. On the other hand, the searches for W'/Z' at the LHC experiments become important for small g_1. The consistencies with these experimental results are telling us information on what type of dynamics is behind the electroweak symmetry breaking. For example, $r \neq 1$ implies parity violating theories unlike QCD-like technicolor models.

We have calculated the signal strength of $gg \to h \to X$ at the LHC and found the Higgs boson at 125 GeV can be partially composite by, for example, 30%, whereas all other constraints are satisfied. If there are significant composite components in the W/Z bosons, the Higgs fields should also be partially composite to reproduce the signal strength measured at the LHC. The deviation from the Standard Model predictions should be visible in future experiments.

[4] In this parameter point, g_1 is larger than 1 but still smaller than $\sqrt{4\pi}$.

ACKNOWLEDGMENTS

We would like to thank Mitsutoshi Nakamura for discussion. R. K. is supported in part by the Grant-in-Aid for Scientific Research No. 23740165 of JSPS.

APPENDIX A: ELIMINATION OF EQ. (14)

In general, the Higgs potential contains the following triple Higgs interaction terms:

$$\kappa_1' \,\mathrm{tr}(H_1 H_2 H_3^\dagger) + i\kappa_2' \,\mathrm{tr}(H_1 H_2 \tau^3 H_3^\dagger). \tag{A1}$$

Note that

$$(\mathrm{tr}(H_1 H_2 H_3^\dagger))^* = \mathrm{tr}(H_1 H_2 H_3^\dagger), \tag{A2}$$

$$(i\,\mathrm{tr}(H_1 H_2 \tau^3 H_3^\dagger))^* = i\,\mathrm{tr}(H_1 H_2 \tau^3 H_3^\dagger). \tag{A3}$$

Hence κ_1' and κ_2' are real numbers. We can rewrite the terms as follows:

$$\kappa_1' \,\mathrm{tr}(H_1 H_2 H_3^\dagger) + i\kappa_2' \,\mathrm{tr}(H_1 H_2 \tau^3 H_3^\dagger) \tag{A4}$$

$$= \kappa \,\mathrm{tr}(H_1 H_2 \exp(i\tau^3\theta_\kappa) H_3^\dagger), \tag{A5}$$

where

$$\kappa = \sqrt{\kappa_1'^2 + \kappa_2'^2}, \quad \cos\theta_\kappa = \frac{\kappa_1'}{\sqrt{\kappa_1'^2 + \kappa_2'^2}}, \quad \sin\theta_\kappa = \frac{\kappa_2'}{\sqrt{\kappa_1'^2 + \kappa_2'^2}}. \tag{A6}$$

By the field redefinition of H_2, we can eliminate $\exp(i\tau^3\theta_\kappa)$, namely

$$H_2 \exp(i\tau^3\theta_\kappa) \to H_2. \tag{A7}$$

This redefinition does not change other terms. Hence we can always eliminate $\mathrm{tr}(H_1 H_2 \tau^3 H_3^\dagger)$.

APPENDIX B: CONSTRAINTS FROM ELECTROWEAK PRECISION MEASUREMENTS

The explicit expressions of self-energies after heavy states are integrated out are

$$\Pi_{W_3W_3}(q^2) = \frac{1}{g_0^2} q^2 - \frac{1}{4}(v_1^2 + v_3^2) - \frac{1}{4} v_1^2 \frac{g_1^2}{q^2 - g_1^2(v_1^2+v_2^2)/4} \frac{1}{4} v_1^2, \tag{B1}$$

$$\Pi_{W_3B}(q^2) = \frac{1}{4} v_3^2 - \frac{1}{4} v_1^2 \frac{g_1^2}{q^2 - g_1^2(v_1^2+v_2^2)/4} \frac{1}{4} v_2^2, \tag{B2}$$

$$\Pi_{BB}(q^2) = \frac{1}{g_2^2} q^2 - \frac{1}{4}(v_2^2 + v_3^2) - \frac{1}{4} v_2^2 \frac{g_1^2}{q^2 - g_1^2(v_1^2+v_2^2)/4} \frac{1}{4} v_2^2. \tag{B3}$$

We introduce the following shorthand notations:

$$\Pi'(0) = \left.\frac{d\Pi(q^2)}{dq^2}\right|_{q^2=0}, \tag{B4}$$

$$\Pi''(0) = \left.\frac{d^2\Pi(q^2)}{d(q^2)^2}\right|_{q^2=0}. \tag{B5}$$

Then we find

$$\Pi_{W_3W_3}(0) = -\frac{1}{4}(v_1^2 + v_3^2) + \frac{1}{4}\frac{v_1^4}{v_1^2+v_2^2}, \tag{B6}$$

$$\Pi'_{W_3W_3}(0) = \frac{1}{g_0^2} + \frac{1}{g_1^2}\frac{v_1^4}{(v_1^2+v_2^2)^2}, \tag{B7}$$

$$\Pi''_{W_3W_3}(0) = 8\frac{1}{g_1^4}\frac{v_1^4}{(v_1^2+v_2^2)^3}, \tag{B8}$$

$$\Pi_{W_3B}(0) = \frac{1}{4} v_2^2 + \frac{1}{4}\frac{v_1^2 v_2^2}{v_1^2+v_2^2}, \tag{B9}$$

$$\Pi'_{W_3B}(0) = \frac{1}{g_1^2}\frac{v_1^2 v_2^2}{(v_1^2+v_2^2)^2}, \tag{B10}$$

$$\Pi''_{W_3B}(0) = 8\frac{1}{g_1^4}\frac{v_1^2 v_2^2}{(v_1^2+v_2^2)^3}, \tag{B11}$$

$$\Pi_{BB}(0) = -\frac{1}{4}(v_2^2 + v_3^2) + \frac{1}{4}\frac{v_2^4}{v_1^2+v_2^2}, \tag{B12}$$

$$\Pi'_{BB}(0) = \frac{1}{g_2^2} + \frac{1}{g_1^2}\frac{v_2^4}{(v_1^2+v_2^2)^2}, \tag{B13}$$

$$\Pi''_{BB}(0) = 8\frac{1}{g_1^4}\frac{v_2^4}{(v_1^2+v_2^2)^3}. \tag{B14}$$

From these results, we find

$$g^{-2}\hat{S} = \Pi'_{W_3B}(0) = \frac{1}{g_1^2}\frac{v_1^2 v_2^2}{(v_1^2+v_2^2)^2}, \tag{B15}$$

$$2g^{-2}m_W^{-2}W = \Pi''_{W_3W_3}(0) = 8\frac{1}{g_1^4}\frac{v_1^4}{(v_1^2+v_2^2)^3}, \tag{B16}$$

$$2g'^{-2}m_W^{-2}Y = \Pi''_{BB}(0) = 8\frac{1}{g_1^4}\frac{v_2^4}{(v_1^2+v_2^2)^3}, \tag{B17}$$

$$g^{-2} = \Pi'_{W_1W_1}(0) = \Pi'_{W_3W_3}(0) = \frac{1}{g_0^2} + \frac{1}{g_1^2}\frac{v_1^4}{(v_1^2+v_2^2)^2}, \tag{B18}$$

$$g'^{-2} = \Pi'_{BB}(0) = \frac{1}{g_2^2} + \frac{1}{g_1^2}\frac{v_2^4}{(v_1^2+v_2^2)^2}. \tag{B19}$$

Final results are given in Sec. III A

APPENDIX C: THEORETICAL CONSTRAINTS ON PARAMETERS IN GAUGE SECTOR

Note that the trace of a mass matrix gives the sum of the masses and the determinant of a mass matrix gives the multiple of the masses, so

$$m_{W'}^2 + m_W^2 = \frac{1}{4}(g_0^2(v_1^2+v_3^2) + g_1^2(v_1^2+v_2^2)), \tag{C1}$$

$$m_W^2 m_{W'}^2 = \frac{1}{16} g_0^2 g_1^2((v_1^2+v_3^2)(v_1^2+v_2^2) - v_1^4). \tag{C2}$$

Using these relations, we find

$$(m_{W'}^2 - m_W^2)^2 = (m_{W'}^2 + m_W^2)^2 - 4m_{W'}^2 m_W^2 \tag{C3}$$

$$= \frac{1}{16}((g_0^2(v_1^2 + v_3^2) - g_1^2(v_1^2 + v_2^2))^2 + 4v_1^4 g_0^2 g_1^2) \tag{C4}$$

$$\geq \frac{1}{4} v_1^4 g_0^2 g_1^2 \tag{C5}$$

$$= 4v_1^4 \frac{m_W^2 m_{W'}^2}{(v_1^2 + v_3^2)(v_1^2 + v_2^2) - v_1^4} \tag{C6}$$

$$= 4m_W^2 m_{W'}^2 \frac{1}{r^2}\left(1 - \frac{v_3^2}{v^2}\right). \tag{C7}$$

Now we derived Eq. (47).

In the $g_1 \gg g_{0,2}$ region, we can easily express v_1 and v_2 as functions of $(m_{W'}, g_1, v, v_3)$ by using Eqs. (16) and (41):

$$v_{1,2}^2 = \frac{2}{g_1^2}\left(m_{W'}^2 \mp \sqrt{m_{W'}^2(m_{W'}^2 - g_1^2(v^2 - v_3^2))}\right). \tag{C8}$$

Here we keep only the leading term in Eq. (41). Since $v_{1,2}$ is real, the $\sqrt{\cdots}$ part should be positive and less than $m_{W'}^2$, and then

$$0 \leq m_{W'}^2 - g_1^2(v^2 - v_3^2) < m_{W'}^2. \tag{C9}$$

From Eq. (16), we find $v^2 > v_3^2$, so the above expression is reduced to

$$g_1^2(v^2 - v_3^2) \leq m_{W'}^2. \tag{C10}$$

Now we have derived Eq. (49).

[1] H. Fukushima, R. Kitano, and M. Yamaguchi, J. High Energy Phys. 01 (2011) 111.
[2] N. Craig, D. Stolarski, and J. Thaler, J. High Energy Phys. 11 (2011) 145.
[3] C. Csaki, Y. Shirman, and J. Terning, Phys. Rev. D **84**, 095011 (2011).
[4] A. Azatov, J. Galloway, and M. A. Luty, Phys. Rev. Lett. **108**, 041802 (2012).
[5] A. Azatov, J. Galloway, and M. A. Luty, Phys. Rev. D **85**, 015018 (2012).
[6] T. Gherghetta and A. Pomarol, J. High Energy Phys. 12 (2011) 069.
[7] J. J. Heckman, P. Kumar, C. Vafa, and B. Wecht, J. High Energy Phys. 01 (2012) 156.
[8] C. Csaki, L. Randall, and J. Terning, Phys. Rev. D **86**, 075009 (2012).
[9] J. L. Evans, M. Ibe, and T. T. Yanagida, Phys. Rev. D **86**, 015017 (2012).
[10] R. Kitano, M. A. Luty, and Y. Nakai, J. High Energy Phys. 08 (2012) 111.
[11] R. Kitano and Y. Nakai, J. High Energy Phys. 04 (2013) 106.
[12] S. Samuel, Nucl. Phys. **B347**, 625 (1990).
[13] M. Dine, A. Kagan, and S. Samuel, Phys. Lett. B **243**, 250 (1990).
[14] R. Harnik, G. D. Kribs, D. T. Larson, and H. Murayama, Phys. Rev. D **70**, 015002 (2004).
[15] E. Witten, Nucl. Phys. **B188**, 513 (1981).
[16] M. Dine, W. Fischler, and M. Srednicki, Nucl. Phys. **B189**, 575 (1981).
[17] S. Dimopoulos and S. Raby, Nucl. Phys. **B192**, 353 (1981).
[18] C. D. Carone and H. Georgi, Phys. Rev. D **49**, 1427 (1994).
[19] E. H. Simmons, Nucl. Phys. **B312**, 253 (1989).
[20] C. D. Carone and M. Golden, Phys. Rev. D **49**, 6211 (1994).
[21] M. Bando, T. Fujiwara, and K. Yamawaki, Prog. Theor. Phys. **79**, 1140 (1988).
[22] M. Bando, T. Kugo, S. Uehara, K. Yamawaki, and T. Yanagida, Phys. Rev. Lett. **54**, 1215 (1985).
[23] M. Bando, T. Kugo, and K. Yamawaki, Prog. Theor. Phys. **73**, 1541 (1985).
[24] M. Bando, T. Kugo, and K. Yamawaki, Nucl. Phys. **B259**, 493 (1985).
[25] B. Bellazzini, C. Csaki, J. Hubisz, J. Serra, and J. Terning, J. High Energy Phys. 11 (2012) 003.
[26] N. Arkani-Hamed, A. G. Cohen, and H. Georgi, Phys. Lett. B **513**, 232 (2001).
[27] R. Contino, Y. Nomura, and A. Pomarol, Nucl. Phys. **B671**, 148 (2003).
[28] R. S. Chivukula, N. D. Christensen, B. Coleppa, and E. H. Simmons, Phys. Rev. D **80**, 035011 (2009).
[29] H. Georgi, Nucl. Phys. **B266**, 274 (1986).
[30] K. Hsieh, K. Schmitz, J.-H. Yu, and C.-P. Yuan, Phys. Rev. D **82**, 035011 (2010).
[31] M. Schmaltz and C. Spethmann, J. High Energy Phys. 07 (2011) 046.
[32] C. Grojean, E. Salvioni, and R. Torre, J. High Energy Phys. 07 (2011) 002.
[33] T. Abe, N. Chen, and H.-J. He, J. High Energy Phys. 01 (2013) 082.
[34] X.-F. Wang, C. Du, and H.-J. He, Phys. Lett. B **723**, 314 (2013).
[35] G. Cacciapaglia, C. Csaki, C. Grojean, and J. Terning, Phys. Rev. D **71**, 035015 (2005).
[36] R. Foadi, S. Gopalakrishna, and C. Schmidt, Phys. Lett. B **606**, 157 (2005).
[37] R. S. Chivukula, E. H. Simmons, H.-J. He, M. Kurachi, and M. Tanabashi, Phys. Rev. D **71**, 115001 (2005).
[38] R. Casalbuoni, S. De Curtis, D. Dolce, and D. Dominici, Phys. Rev. D **71**, 075015 (2005).
[39] R. S. Chivukula, E. H. Simmons, H.-J. He, M. Kurachi, and M. Tanabashi, Phys. Rev. D **72**, 015008 (2005).

[40] R. Barbieri, A. Pomarol, R. Rattazzi, and A. Strumia, Nucl. Phys. **B703**, 127 (2004).
[41] ATLAS Collaboration, Report No. ATLAS-CONF-2013-015.
[42] CMS Collaboration, Phys. Rev. Lett. **109**, 141801 (2012).
[43] ATLAS Collaboration, Eur. Phys. J. C **72**, 2241 (2012).
[44] CMS Collaboration, Report No. CMS-PAS-EXO-12-060.
[45] ATLAS Collaboration, Report No. ATLAS-CONF-2013-017.
[46] CMS Collaboration, Report No. CMS-PAS-EXO-12-061.
[47] J. Pumplin, D. R. Stump, J. Huston, H. L. Lai, P. M. Nadolsky, and W. K. Tung, J. High Energy Phys. 07 (2002) 012.